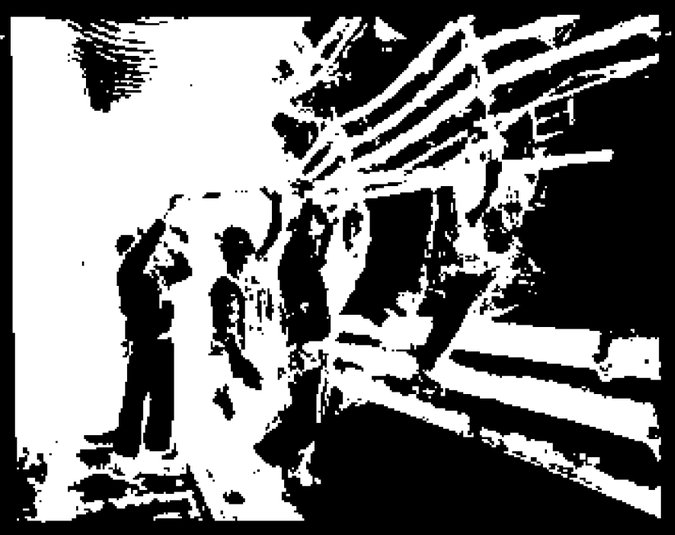

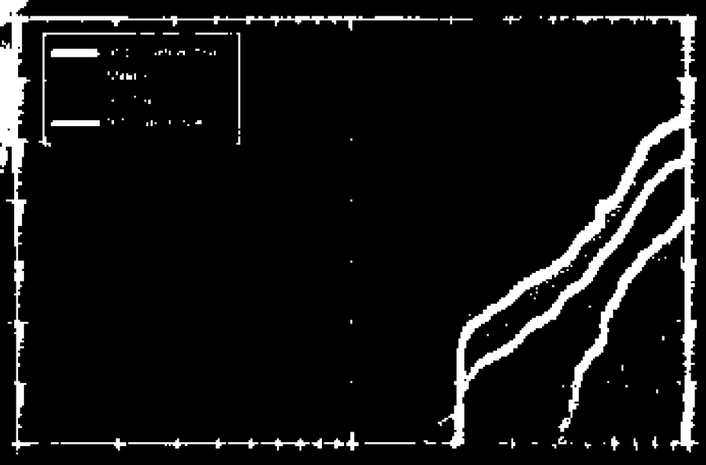

FY01 Supplemental Science and Performance Analyses,

Volume 1: Scientific Bases and Analyses

Part 1 of 2

U.S. Department of Energy
Office of Civilian Radioactive Waste Management

June 2001

Near the waste emplacement drifts, the natural system would be perturbed by the mechanical excavation of the drifts and by the heat generated by radioactive decay in the emplaced waste. The heat and the mechanical stresses could affect the natural processes in complex ways. The coupling of these natural and man-made processes may introduce additional complexity into models of repository performance. Therefore, the S&ER (DOE 2001 [DIRS 153849]) also explains how these coupled thermal-hydrologic-geochemical-mechanical processes would be likely to affect the long-term performance of the repository. These processes affect both the natural and the engineered barriers, including the drip shields, the waste forms, the waste packages, and the invert below the waste packages. In addition to the hydrologic and geochemical processes that would act in and around the potential repository, disruptive events, such as the possibility of volcanic eruptions, could affect the integrity of the repository. The S&ER describes the likelihood and consequences of disruptive events at Yucca Mountain.

The S&ER (DOE 2001 [DIRS 153849], Section 4.4) summarizes the results of a comprehensive quantitative analysis of the possible future behavior of a Yucca Mountain repository. This analysis, known as the *Total System Performance Assessment for the Site Recommendation* (TSPA-SR) (CRWMS M&O 2000 [DIRS 153246]), combines the results of detailed conceptual and numerical models of each of the individual and coupled processes in a single probabilistic model that can be used to assess how a repository might perform over long periods of time.

Despite the extensive scientific studies described in the S&ER (DOE 2001 [DIRS 153849]), the DOE has always recognized that significant uncertainties will remain in any assessment of the performance of a repository over thousands of years, as discussed in the S&ER (DOE 2001 [DIRS 153849], Sections 1.5, 4.1, and 4.4). These uncertainties are attributable to a variety of causes, ranging from uncertainty regarding the fundamental processes that may affect radionuclide migration to uncertainty related to the design and operation of the potential repository. For this reason, one part of the DOE approach to dealing with uncertainty relies on multiple lines of evidence that may contribute to the understanding of the performance of the potential repository. Another part of the DOE approach is a commitment to continued testing, monitoring, and analysis beyond the possible recommendation of the site.

This report has been prepared to address several specific aspects of the existing uncertainties related to the performance of a potential Yucca Mountain repository. It describes new information developed since the completion of the S&ER (DOE 2001 [DIRS 153849]) and its key supporting references, the TSPA-SR (CRWMS M&O 2000 [DIRS 153246]) and the analysis model reports and process model reports cited therein.

Uncertainties in mountain-scale flow (including gas convection, liquid flow focusing, and diversion) contribute to uncertainties in mountain-scale THC processes. Other uncertainties include thermodynamic and kinetic data of vitric and zeolitic tuffs, precipitating mineral assemblages, effective mineral-water reactive areas in heterogeneous unsaturated fracture rocks, fracture and lithophysal hydrologic properties, and distributions of water and gas chemistry in the UZ and in the infiltrating water. Sensitivity studies were conducted to understand the impact of THC processes on the mineral changes during thermal periods in the zeolitic CHn, on matrix porosity reduction in the TSw, on enhanced precipitation at the edges of the potential repository block with gas convection, and on many other THC effects. The modeling approach and uncertainties for THC effects on mountain-scale flow and geochemistry in both AMR revisions and recent evaluations are discussed in detail in Section 3.3.6.

3.2.7 Thermal-Hydrologic-Mechanical Effects on Mountain-Scale Flow

Process Description–A new coupled thermal-hydrologic-mechanical (THM) model is developed to calculate the impact of THM processes on flow at the mountain scale. Two well-established codes, TOUGH2 V1.5 for TH processes and FLAC 3D V2.0 for mechanical processes, are coupled together through carefully designed linkage routines. Four types of conservation equations are solved, including two mass-balance equations for the two fluid (liquid and gas) components, one energy (heat) balance equation, and one momentum conservation equation for the rock deformation forces. The mechanical behavior of porous and fractured media responds to changes in temperature, in effective stress, and in strain, resulting in permeability, porosity, and flow-field changes.

Current Modeling Approach and Uncertainties–A two-dimensional model is constructed with vertical layering extended from the ground surface to the water table. Laterally, the model extends from the centerline of the potential repository to a far-field outer boundary located at distance of 5,000 m to the east, over twice the radius of waste emplacement area (2,160 m). The thermal loading, ventilation period, and heat removal efficiency are the same as the values used by the mountain-scale TH model.

Uncertainties in the TH model contribute to uncertainties in THM model. Similar to any newly developed model, uncertainties are relatively large and require substantial input data to conduct the calibration, validation, and thereby build confidence in the models. Calculated changes of permeability depend on such factors as rock stiffness parameters and residual permeability values, heterogeneity of hydrologic and mechanical properties, boundary conditions, dimensionality of the model, and realistic geometries. Geotechnical engineering field and laboratory studies are needed to quantify the uncertainties of THM impact. The modeling approach and uncertainties for THM effects on mountain-scale flow in recent evaluations are discussed in detail in Section 3.3.7.

approach was chosen because it provides the means to test the appropriateness of the conceptual model, to evaluate uncertainties in different conceptual models, and to provide predictions of potential effects on water and gas chemistry, as well as changes in hydrologic properties that result in changes in flow. Uncertainties in some thermodynamic and kinetic parameters were evaluated using sensitivity studies and comparisons to data from the Drift Scale Test and laboratory experiments, which are discussed in Section 4.3.6. Remaining unquantified uncertainties were addressed in *Features, Events, and Processes in UZ Flow and Transport* (BSC 2001 [DIRS 154826]). Unquantified conceptual uncertainties were assessed in analogue studies and other corroborating observations (CRWMS M&O 2000 [DIRS 141407]).

The conceptual model for THC processes provides a framework for modeling the pertinent mineral-water-gas reactions in the host rock, under thermal loading conditions, as they influence the chemistry of water and gas in the mountain and associated changes in mineralogy. The data incorporated in the model include hydrologic and thermal properties from the calibrated property sets, geologic layering from the UZ three-dimensional flow and transport model, geochemical data (fracture and matrix mineralogy, aqueous geochemistry, and gas chemistry) derived from various sources, thermodynamic data (minerals, gases, and aqueous species), data for mineral-water reaction kinetics, and transport data. Simulations of THC processes included coupling among heat, water, and vapor flow; aqueous and gaseous species transport; kinetic and equilibrium mineral-water reactions; and feedback of mineral precipitation/dissolution on porosity, permeability, and capillary pressure for a dual-permeability (fracture-matrix) system.

The effect of coupled THC processes on the evolution of flow fields and water and gas chemistry in the UZ is evaluated in this section for a higher-temperature thermal operating mode based on the thermal loading and properties used in *Mountain-Scale Coupled Processes (TH) Models* (CRWMS M&O 2000 [DIRS 144454]). Because this is a new model, a higher-temperature baseline analysis was performed first, which may bound the upper limit of THC effects on mountain-scale flow and chemistry that may be expected under above-boiling conditions. Effects of THC processes at the drift scale under the lower-temperature operating mode are evaluated in Sections 4.3.6 and 6.3.1.5.

3.3.6.2 Goal of the Mountain-Scale Thermal-Hydrologic-Chemical Model

The goals of the model used for prediction of mountain-scale THC processes are:

- Provide a conceptual basis and methodology for developing a mountain-scale THC model to assess uncertainties in the modeling results. Use the results to assess uncertainties in the drift-scale THC models (as well as other UZ flow and transport models)

- Predict large-scale changes in hydrologic properties resulting from mineral precipitation/dissolution and associated THC effects on UZ flow

- Predict large-scale mineralogic changes that could impact UZ transport (i.e., effects on glassy and zeolitic units below the potential repository) (see Section 11.3.5)

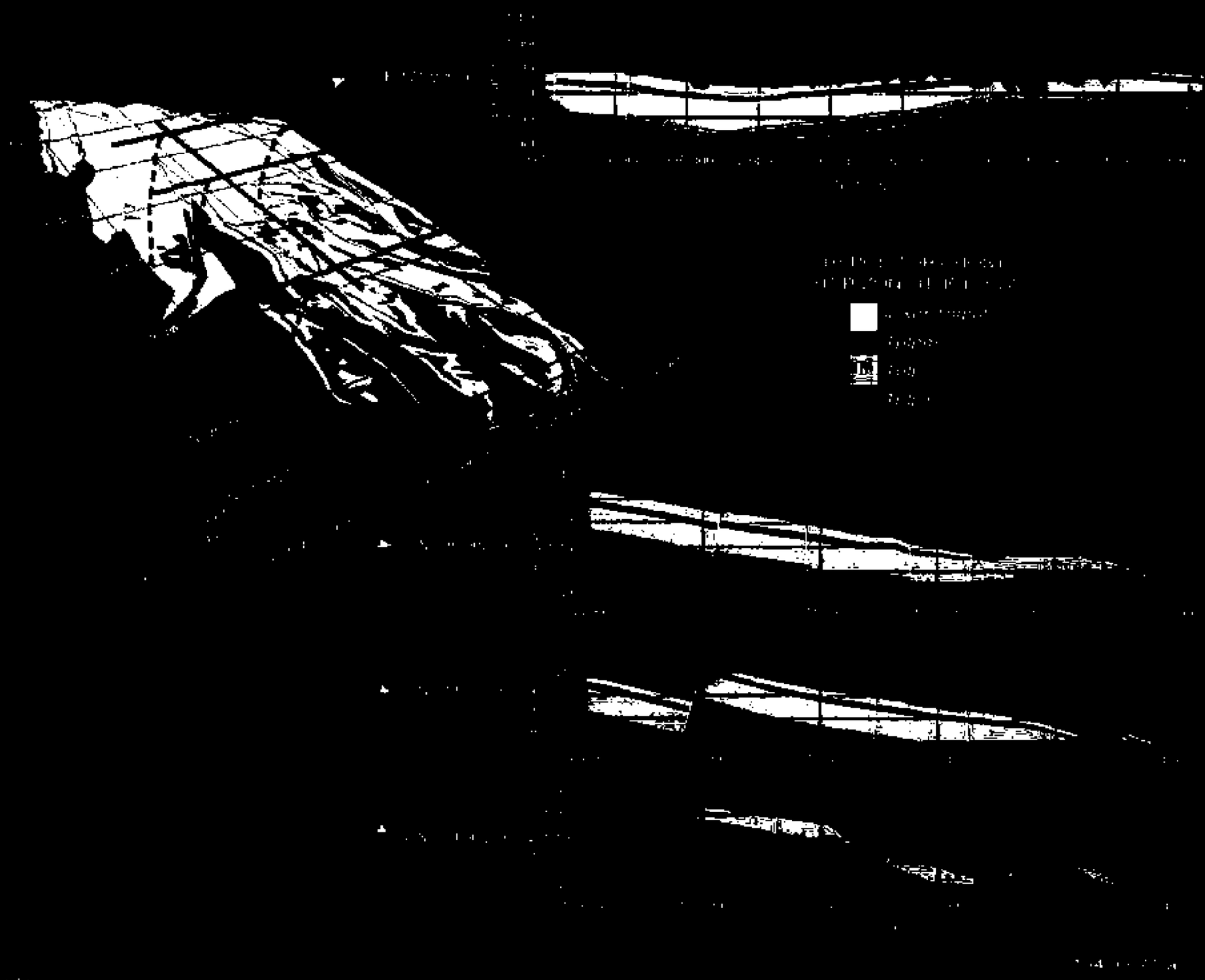

Source: Developed from DTN: MO9901MWDGFM31.000 [DIRS 103769]

NOTE: Upper and lower repository host horizon surfaces have been capped to maintain an overburden thickness of 200 m and a water table standoff distance of 160 m. Nevada coordinates in meters.

Figure 3.3.4-9. Spatial Distribution of Lithostratigraphic Layers Constituting the Potential Repository Host Horizon

Section 6.4). This approach yielded flow focusing up to a factor of 47 (CRWMS M&O 2000 [DIRS 142004], Section 6.4). This section describes an intermediate-scale model that bridges that gap specifically to address the issue of spatial flow focusing. The effects of faults on flow focusing are not included because of the scale used in the modeling studies.

To quantify flow focusing and address the uncertainty associated with the estimation of flow focusing factors, a stochastic fracture continuum model was developed that honors fracture data from welded tuffs by using measured fracture permeability data. This model was used to study flux allocation mechanisms and flow patterns. It was also used to assess the frequency and flux distributions of major water-bearing flow paths and transport pathways from the bottom of the PTn to the potential repository horizon.

The flow focusing factor (the ratio of local flux to average percolation flux) evaluated in this section is used to determine the upper (spatially variable) boundary flux of the drift-scale model by sampling from the frequency distribution of the flow focusing factor. The modeling results in this section indicate that the flow focusing factors currently used in the TSPA models are very conservative.

4.3.2.2 Goal of the Heterogeneous Flow Model for Site-Scale Domains

Flow focusing along preferential paths, such as well-connected fracture networks, may control patterns of percolation through the highly fractured TSw and directly affect seepage into emplacement drifts. The detailed mechanisms that control unsaturated flow and transport in fractured rocks are site-specific and difficult to characterize. Accurate description of flow focusing processes in unsaturated fractures may be important for the detailed prediction of flow patterns or water seepage into the potential emplacement drifts. However, knowing uncertainty ranges and the average behavior of flow focusing and discrete paths may be more important to the TSPA calculations. This section addresses uncertainties from earlier studies that did not provide sufficient detail on fracture flow at the necessary scale. In addition, drift-scale modeling studies on seepage into drifts show that the amount of water that bypasses or breaks through a capillary barrier of a drift wall depends not only on the capillarity and permeability of the surrounding fracture system, but also on the heterogeneity of the water flux and flow paths (CRWMS M&O 2001 [DIRS 153045], Section 6.1.5).

Various conceptual models have been proposed for describing water flow through the thick, fractured UZ at Yucca Mountain. These models range from continuous flow through a well-connected fracture network (e.g., CRWMS M&O 2000 [DIRS 122797]) to sparse, discrete flow through a small fraction of the fracture network (Pruess et al. 1999 [DIRS 117112]). Modeling approaches used to characterize fracture flow include:

- Continuum modeling (e.g., the effective continuum model) and dual-permeability modeling (Wu et al. 1999 [DIRS 117161]).
- Stochastic modeling representing discrete fractures as currently applied to drift-scale processes (Finsterle 2000 [DIRS 151875]).

4.3.6.7 Multiple Lines of Evidence

The emplacement of heat-generating nuclear waste in a potential geologic repository at Yucca Mountain will result in enhanced water-rock interaction around the emplacement drifts compared to the rates of reaction occurring under ambient conditions. As the waste package heats the surrounding environment, water present in the matrix and fractures of the nearby rock may vaporize and migrate through fractures to cooler regions where condensation would occur. The condensate would dissolve gases and minerals, and mineralized water flowing under gravity back towards the heat source would evaporate, depositing the dissolved minerals. Such mineral deposition would reduce porosity and permeability above the potential repository, thus altering the flow paths of percolating water (Nitao and Glassley 1999 [DIRS 154486]). Natural analogue studies of water-rock interaction in geothermal systems and along igneous contacts, as well as hydrothermal field and laboratory experiments, provide multiple lines of evidence for THC effects on permeability and porosity that would change seepage (Apps 1995 [DIRS 154615]). A number of natural analogue examples and field and laboratory studies are summarized below, followed by a more detailed examination of the Yellowstone geothermal system and a tuff dissolution-precipitation experiment. The processes demonstrated by these examples are then related to Yucca Mountain, with an emphasis on how differences in scale could influence the impact that these processes may have on the performance of the potential repository.

4.3.6.7.1 Effects of Water-Rock Interaction on Fluid Flow: Natural Analogues

The effects of water-rock interaction on important hydrogeological properties, such as permeability and porosity, have been widely documented for a number of geologic settings. Geothermal systems and igneous contacts, such as those discussed below, illustrate how heat and water can cause mineral dissolution and precipitation, resulting in changes in formational fluid flow properties. Water-rock interaction tends to be more extensive in long-lived, water-saturated geothermal systems than along shallow intrusive and extrusive contacts occurring above the water table, where short-lived thermal perturbations provoke minimal mineralogic changes. These geologic systems encompass the time scales and heterogeneities necessary to evaluate models for the potential Yucca Mountain repository and provide important information needed to build, calibrate, and evaluate numerical models for the Yucca Mountain system. Three geothermal systems and three magmatic contact areas are summarized in the following paragraphs.

Imperial Valley Geothermal Fields, California–The effects of water-rock interaction have been studied at a number of geothermal fields (Salton Sea, East Mesa, Heber, Brawley, Cerro Prieto, and the Dunes) within the Imperial Valley (e.g., Schiffman et al. 1985 [DIRS 154644]; Cho et al. 1988 [DIRS 154599]). Elders (1987 [DIRS 154632]) examined the Salton Sea geothermal field as a potential natural analogue for evaluating processes related to radioactive waste storage. Low-permeability carbonate-cemented sandstones form the primary caprock, and represent the first of four distinct hydrothermal alteration zones. Fractures provide fluid flow pathways that cut across low-permeability shale interbeds. Complex sequences of fracture mineralization observed at the Salton Sea indicate that fractures episodically opened and sealed throughout the life of the geothermal system (Elders 1982 [DIRS 154602]). Silica sealing has been documented at the Dunes geothermal system (Bird and Elders 1976 [DIRS 154601]). Seven distinct zones of sandstones and conglomerates located in what originally were the most

Source: Bodvarsson 2001 (DIRS 154669), Attachment 16, p. 12 and data files listed on p. 11.

NOTE: Simulated using the base case scenario, correlation length = 1 m, infiltration = 5 mm/yr, (a) at a depth of 25 m or (b) at the bottom.

Figure 4.3.2-2. Distribution of Vertical Fluxes within the Two-Dimensional Model Domain

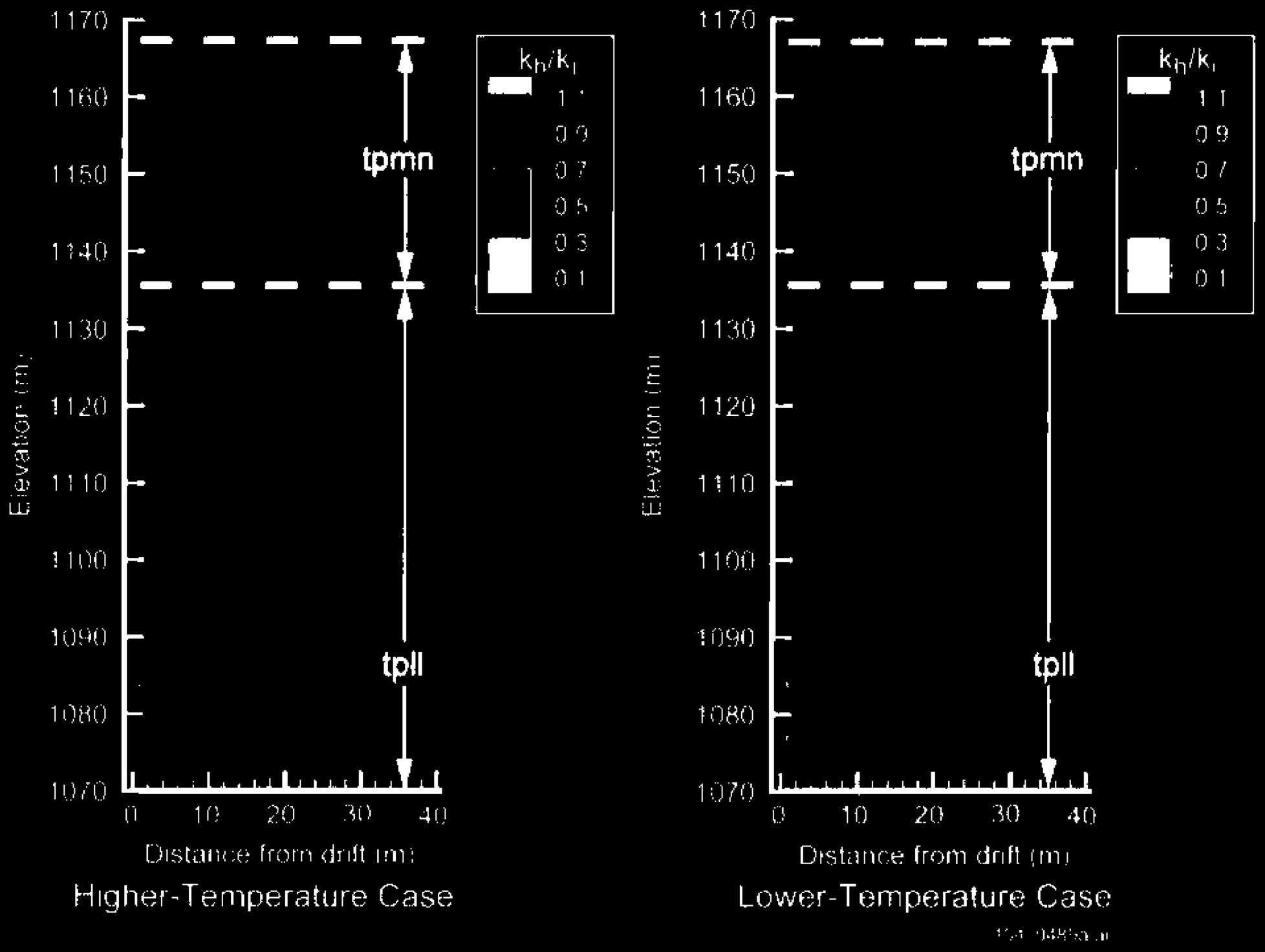

Source: Bodvarsson 2001 [DIRS 154669], Attachment 9, pp. 57 to 74

Figure 4.3.7-12. Horizontal Permeability Changes at 10 Years

The sensitivity of the MSTH model liquid saturation in the invert material was also evaluated for the LTOM. Figure 5.3.1.4.7-4 shows the predicted liquid saturation at the same location in the potential repository footprint as the temperature and relative humidity assessments discussed above. The results are for the upper invert layer directly below the drip shield, in the central portion of the drift (Figure 5.3.2.3-1). These analyses were performed for the mean infiltration flux case. The onset of rewetting occurs earlier in the invert for the LTOM than for the HTOM (compare Figures 5.3.1.4.7-4 and 5.3.1.4.7-2). The same trends between the permeability cases are observed in the LTOM as in the HTOM. The general trend is that the onset of rewetting increases with permeability and that the final "steady-state" value of liquid saturation increases with decreasing permeability. Because the capillary properties of the fractures were not varied along with the permeability of the fractures and because a single continuum was used to represent the crushed-tuff invert, the trend between these k_b cases should be viewed qualitatively rather than quantitatively.

Comparison of Results of Higher- and Lower-Temperature Operating Modes-Peak temperatures on the drift wall in the central portion of the potential repository for the HTOM and the LTOM are about 144 and 74°C, respectively; under mean infiltration and mean permeability conditions for the MSTH submodel. The temperatures decrease to ambient (i.e., approximately 22.5°C for the glacial climate) around 100,000 years. The relative humidity on the drift wall for the HTOM drops to about 20 percent about 10 years after closure, then increases to nearly 100 percent at about 1,000 years. The temperatures at the time that the drift wall relative humidity approaches 100 percent are about 90°C, and decrease to 70°C around 4,000 years. Thus, there is a period of about 3,000 years when the relative humidity is nearly 100 percent and temperatures are higher than 70°C. For the LTOM, the relative humidity is always nearly 100 percent. The drift wall temperatures for the LTOM are between 70 and 74°C from about 400 to 1,500 years. Thus, there is a period of about 900 years when the temperatures are slightly above 70°C and the relative humidity is nearly 100 percent.

Summary-Uncertainty in the values of bulk permeability that were used as inputs to the MSTH model, as evaluated in the sensitivity studies of two standard deviations from the mean value, had very little effect on the temperature and relative humidity at the drift wall and drip shield for the HTOM and LTOM. Liquid saturation in the invert has the same weak dependence on bulk permeability for the HTOM and the LTOM. The general trend is that the onset of rewetting increases with permeability and that the final "steady-state" value of liquid saturation increases with decreasing permeability. Because the capillary properties of the fractures were not varied along with the k_b of the fractures and because a single continuum was used to represent the crushed-tuff invert, the trend between these k_b cases should be viewed qualitatively rather than quantitatively.

5.3.1.4.8 Sensitivity to Host Rock Thermal Conductivity

Sensitivity analyses were performed to consider the uncertainties in drift-wall and drip-shield temperature, and relative humidity, and invert liquid saturation that result from uncertainties in the values of host rock thermal conductivity used in the MSTH model. Section 5.3.1.4.11 discusses the Waste Package temperatures and relative humidities. The MSTH model uses values of bulk host rock thermal conductivity as input. In field and laboratory measurements of host-rock thermal conductivity used in these thermal-hydrologic calculations, there is not

Since the invert temperature is an average through its half-depth, its surface is hotter than either its average or the drip shield surface. Thus, for the natural convection (perimeter-averaged) correlation and the low value of invert thermal conductivity used in the calculation, condensation would be favored on the drift wall near the coolest waste package. However, condensation depends on surface conditions as well as temperature; thus the temperature relationships are not enough to draw conclusions about condensate geometry on rock, titanium, and gravel.

Airflow patterns of natural convection are expected to shift the temperature of the drip shield (upper region) upward and the temperature of the invert surface under the drip shield downward. Therefore, natural convection could result in a cooler invert than the drip shield, reducing potential condensation on the underside of the drip shield. As corroboration of this logic, observations of the quarter-scale canister test were that the invert was cooler than the drip shield, with no dripping or rivulets observed under the drip shield (Howard et al. 2001 [DIRS 153282]).

Table 5.3.2.4.6-2 illustrates the temperatures in five cross-sections through the ten waste package computational cell for the LTOM. The cell includes the same sequence of waste packages as for the HTOM. However, there are variable length gaps between the waste packages with the goal of smoothing the local lineal heat loading. This geometric smoothing is an alternative to the axial radiation heat transfer between waste package ends that smoothes the local lineal heat loading in the HTOM. The five cross-sections are through the mid-lengths of the hottest waste package (PWR), an average power waste package (BWR), a cool waste package (DHLW), a warm gap, and a cool gap between waste packages. The times selected include the time of peak preclosure temperature, just after closure, three times representing the broad period of near-peak postclosure temperature, during the slow cooling of the potential repository (as the waste decays), and a final time at which near-ambient temperatures have been reached.

During the preclosure period, the low relative humidity of the ventilation air will limit the water content of the in-drift air enough that water films will be negligible. Under some conditions, highly deliquescent salts in dust on some components may be able to cause condensation at low humidity; these conditions are being studied in support of a potential license application. As soon as ventilation ceases for the LTOM, all temperatures are sufficiently low that condensate could form.

At the time of peak waste package temperature, the range of temperature differences on all surfaces within the three-dimensional cell is about 10°C. Within a cross section, the range is as little as 1°C at the cool waste package to as much as 8°C at the design basis (hottest) waste package. Along the drift axis, the range is about 2°C at the drift wall, and about 9°C at the waste package. Thus, the axial range is similar to the range within a cross section.

As temperatures cool, the coolest surfaces in the drift are at the drift wall. The invert zone under the drip shield is slightly warmer than the drip shield itself. Because the invert temperature is an average through its half-depth, the surface is hotter than either the average or the drip shield surface. As for the HTOM, shifts in temperature patterns around the perimeter of air flow loops could reverse the temperature relationship between the drip shield and invert surface, resulting in little condensation on the drip shield underside.

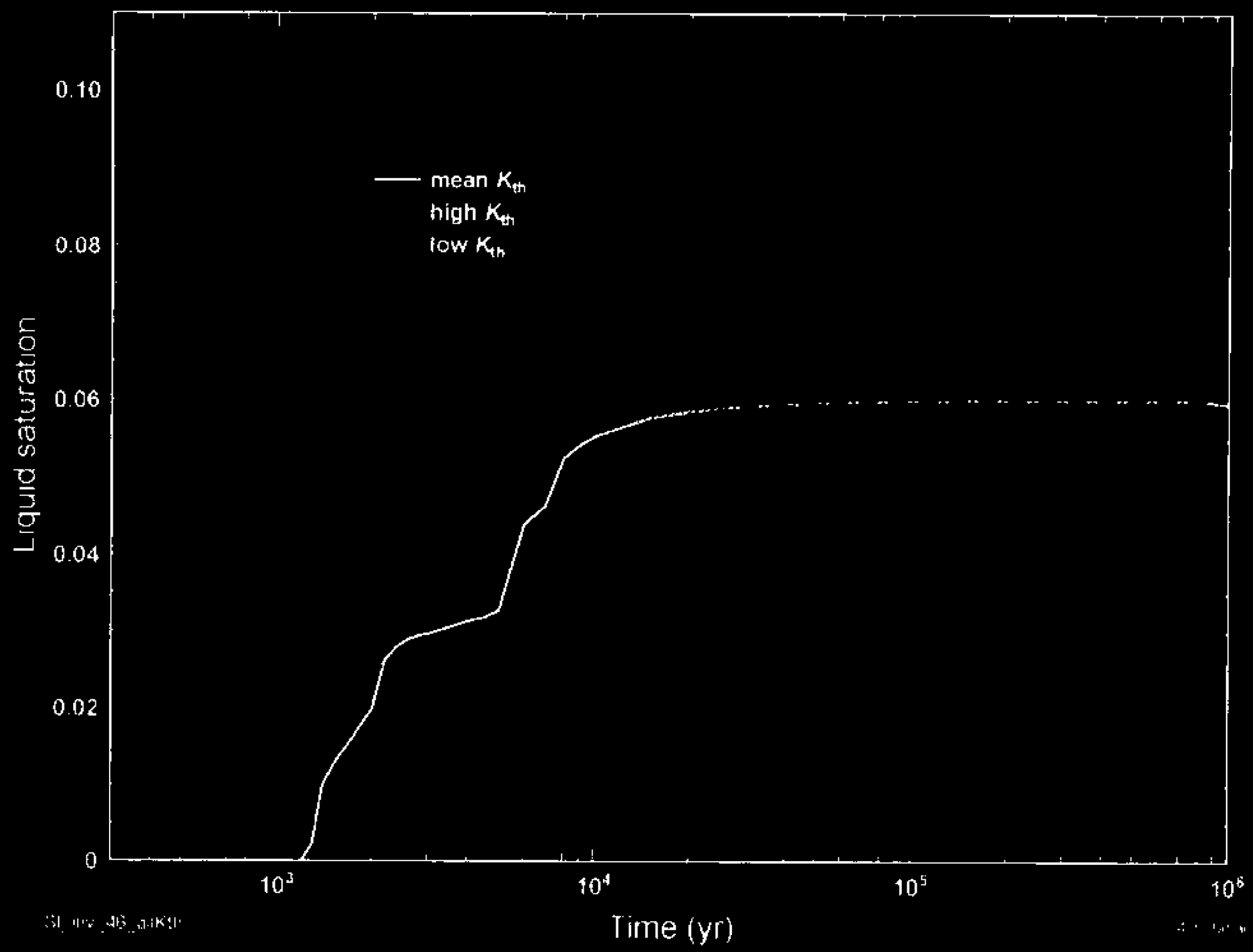

Source: Produced using files from Buscheck 2001 [DIRS 155012]

Figure 5.3.1.4.8-4. Liquid-saturation in the Invert as a Function of Host-Rock Thermal Conductivity for the Central Repository (L5C3) Location of the Lower-Temperature Operating Mode and the Mean Infiltration-Flux Scenario

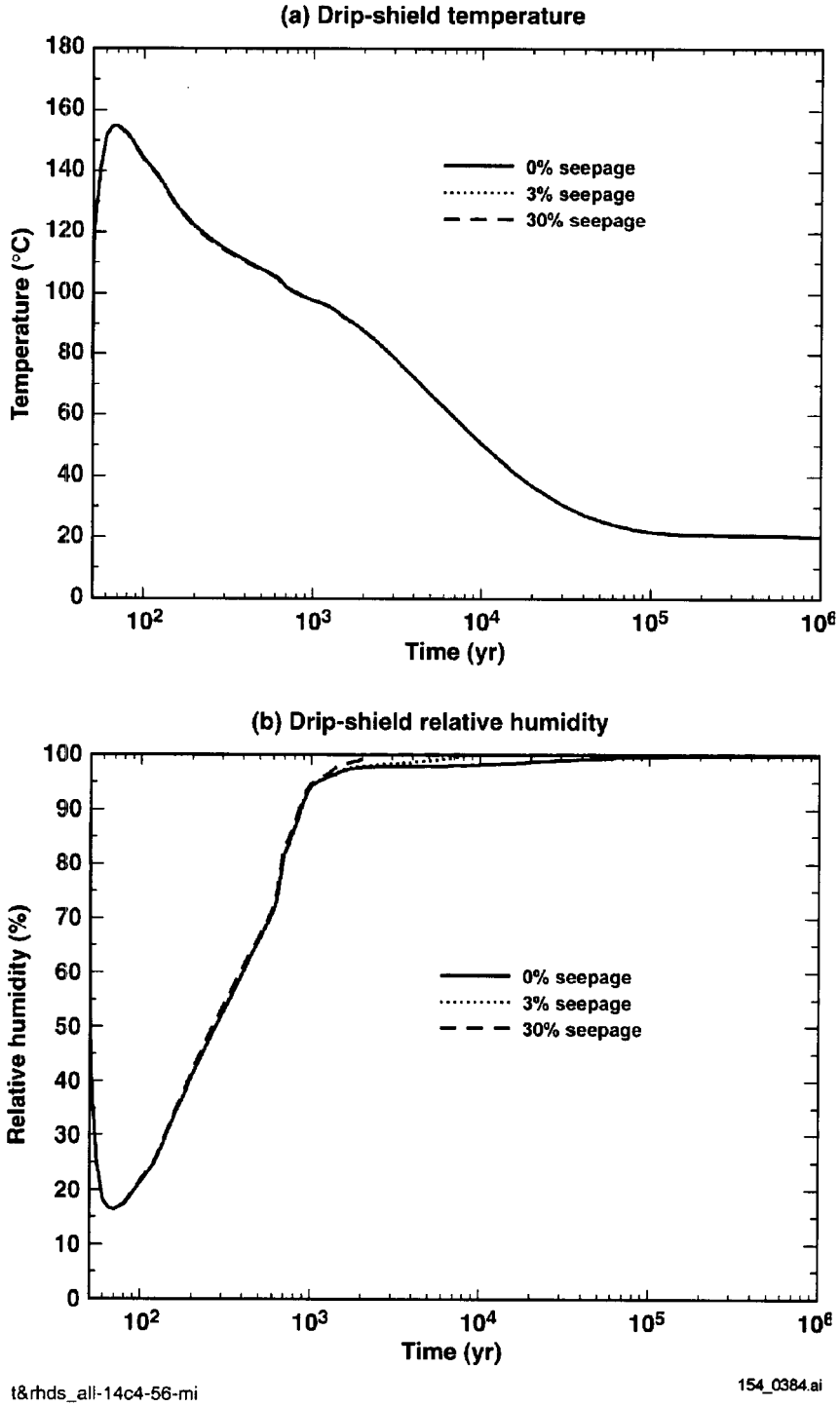

Source: Produced using files from Buscheck 2001 [DIRS 155012], Figure 6-34.

Figure 5.3.2.4.4-7. Temperature (a) and Relative Humidity (b) Histories at the Drip Shield for 0 Percent, 3 Percent, and 30 Percent of the Percolation Flux Seeping into the Drift

dioxide gas and reactive aqueous species such as calcium, magnesium, and sodium by several orders of magnitude (see Section 6.3.1.4).

The initial THC seepage model (CRWMS M&O 2000 [DIRS 142022]) was also useful to evaluate the effect of infiltration on computed water and gas compositions around drifts because a wider range of infiltration rates was considered than in subsequent work (BSC 2001 [DIRS 154677]). Three infiltration rate scenarios were considered, each with varying infiltration over time to simulate future wetter conditions: a mean case (rates between 6 and 25 mm/yr), an upper-bound case (rates between 15 and 47 mm/yr), and a lower-bound case (rates between 0.6 and 6 mm/yr). A fixed ambient mean infiltration rate near 1 mm/yr was also considered for ambient THC simulations.

The different infiltration cases did not significantly affect predicted trends of temperature at the wall of the modeled drift, with no more than an approximately 15 percent temperature variation (under thermal load) between the lower-bound and upper-bound infiltration cases. A similar conclusion was reached for the *Multiscale Thermohydrologic Model* (CRWMS M&O 2000 [DIRS 149862], Sections 6.11.1.4, 6.11.2, 6.11.3.2, and 6.11.4.2), and the *Water Distribution and Removal Model* (CRWMS M&O 2001 [DIRS 152016], Sections 6.3.3.1 and 6.3.3.2).

During the cooling phase, significant fluid composition differences were predicted around the drift between the lower-bound and the mean infiltration cases (up to 1.5 pH units and nearly two orders of magnitude carbon dioxide concentration). Such large differences were not observed between the mean and upper-bound infiltration cases (mostly within half an order of magnitude). As previously, these simulations were affected by overly reactive aluminosilicate minerals, which likely exacerbated the predicted concentration differences between the lower-bound and mean infiltration cases. As infiltration rates increase, advective rates (i.e., seepage velocity) increase relative to reaction rates, such that calculated concentrations become more dependent on advective rates than on reaction rates (and less sensitive to the latter).

The probability of seepage into drifts increases with increasing infiltration rates. However, as infiltration rates increase, the effect of mineral reactions on water composition decreases (at least for minerals with slow reaction rates such as aluminosilicate minerals), and the assumed composition of infiltration waters and gases becomes important in determining the composition of fluids that may enter drifts. Therefore, in this respect, uncertainties on the assumed composition of infiltrating water should largely dominate the effect of uncertain infiltration rates. In addition, if uncertainties in reaction rates can be minimized through a justifiable calibration of thermodynamic and kinetic data to the initial (measured) water composition, as was done for the revised THC simulations (BSC 2001 [DIRS 154677]) (see Section 6.3.1.4), the assumed composition of initial pore water and infiltration water input into the model (and associated carbon dioxide partial pressures) become among the main model uncertainties regarding predicted water compositions.

To summarize, the initial THC seepage model (CRWMS M&O 2000 [DIRS 142022]) is useful to semiquantitatively evaluate the model sensitivity to the reaction rates of aluminum silicate minerals and to a range of infiltration rates including future climates wetter than the present day. However, under high infiltration rate conditions most favorable to in-drift seepage, uncertainties in these parameters are likely to be overshadowed by the assumed composition of fluids

The EQ3N/R (EQ3/6 V7.2b) runs produced pickup files that initialized sets of EQ6 runs designed to evaporate water (remove water) incrementally, precipitate supersaturated unsuppressed minerals, and equilibrate the solution with the fugacity of carbon dioxide of the crown for the corresponding time period and thermal/carbon dioxide mode. Reaction progress was limited to that required to produce an activity of water of 0.85, which corresponds to an aqueous solution equilibrated with air having a relative humidity of 85 percent. At this activity, ionic strength ranges between about 4 and 10 molal, depending on the dominant ions and pH. The pickup files from these runs were then used to initialize solid-centered flow-through EQ6 calculations in which both seepage and evaporation occur. The ratio of evaporation rate to seepage rate was varied from –9.0 to 0.999 to cover all realistic possibilities for this ratio. The value of –9.0 represents condensation (negative evaporation) at a rate that is 9 times that of seepage, while the value of 0.999 represents an evaporation rate that is 99.9 percent of the seepage rate. In some cases, the latter value resulted in water activity values less than 0.85, so the ratio was reduced to prevent the activity from exceeding 0.85. These runs generated steady-state water compositions that were independent of the starting solution (CRWMS M&O 2001 [DIRS 153265]). For each ratio of evaporation rate to seepage rate, steady-state results were added to the lookup tables. These results included pH, ionic strength, the molalities of each component, and the molalities of a set of aqueous species that potentially contribute to alkalinity. An example lookup table for the subset of output parameters is presented in Table 6.3.3-1.

For precipitates/salts model results at relative humidity values less than 85 percent, the low relative humidity model was used, following the same procedure outlined in *In-Drift Precipitates/Salts Analysis* (CRWMS M&O 2001 [DIRS 153265]). It was used to predict pH, ionic strength, and chloride concentration as a function of relative humidity. These predictions were also added to each lookup table and to the example in Table 6.3.3-1. The complete set of lookup tables and supporting model input and output files were transmitted to the TSPA implementation team (Jolley 2001 [DIRS 154762]).

The results show some new trends for pH compared to the trends observed in the calculations performed for the TSPA-SR (CRWMS M&O 2000 [DIRS 153246]). Unlike the previous boiling period predictions, where the pH increased above 9 (CRWMS M&O 2001 [DIRS 153995], Figure 2), the preliminary performance assessment pH calculations never increase much above 8. The pH instead generally remains in the range of 6.5 to 8, except during the thermal periods of the higher-temperature scenarios. Under these conditions, the pH falls to around 5 or slightly lower as evaporation produces ionic strengths above 1 molal. These lower pH predictions are caused by the differences in the abstracted seepage and gas compositions used as input. The changes in these abstracted input compositions are discussed at length in Section 6.3.1.

Predictions of the chloride and ionic strength do not show new trends. Their molalities increase in approximately the same proportions as previously observed when relative humidity decreases and ratios of the rates of evaporation and seepage increase (CRWMS M&O 2001 [DIRS 153995]). However, as discussed in Section 6.3.3.5.1.1, the results of the high relative humidity model show that during the thermal period, a calcium chloride brine could possibly develop due to predicted chemical divides and the excess of chloride in the seepage water during the thermal periods. This possibility is not captured in the low relative humidity model results for chloride concentration or in the relative humidity threshold assumption, which assumes dry

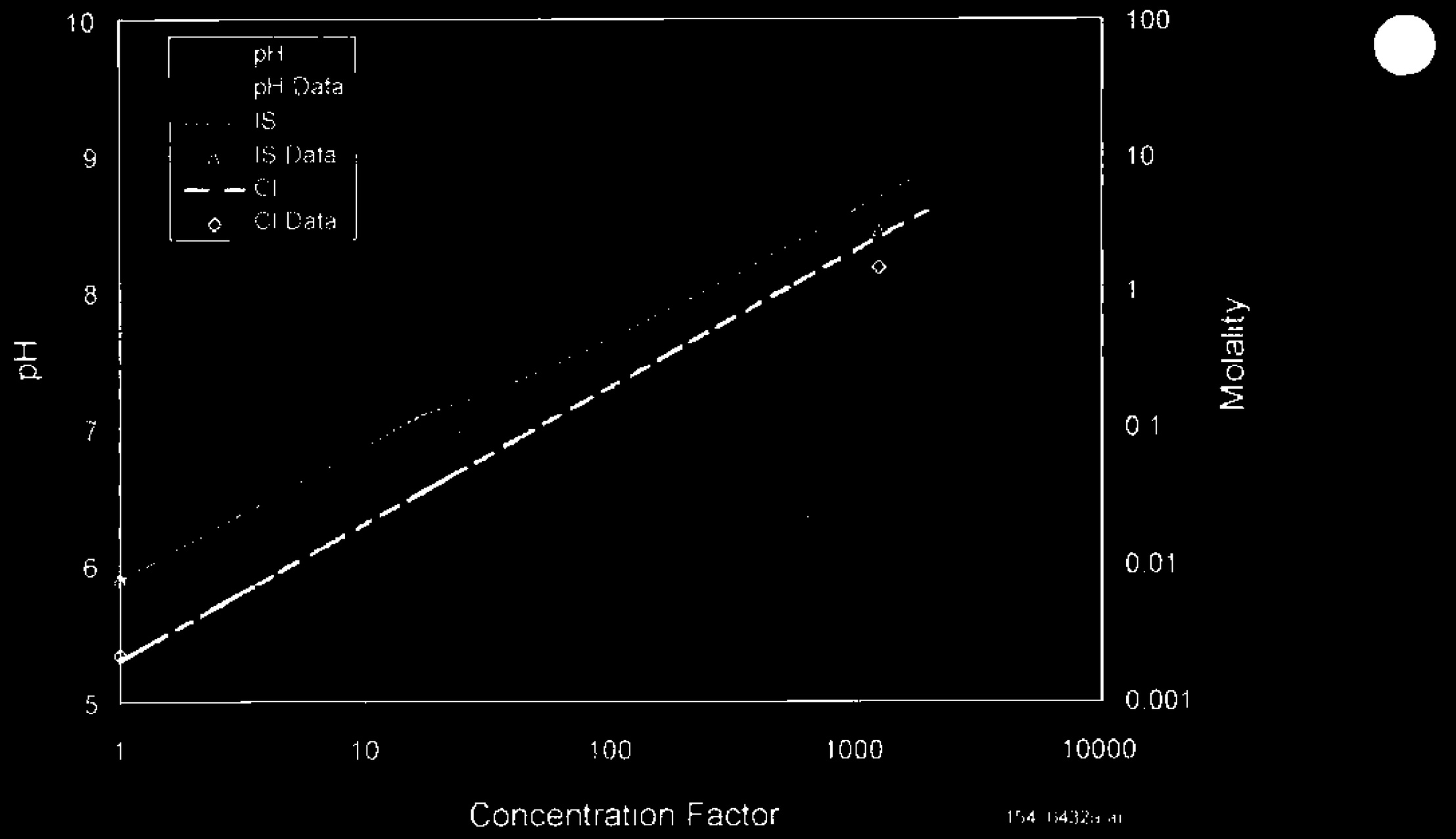

Source: Data from Rosenberg et al. 1999 [DIRS 125339]; Model predictions from Jolley 2001 [DIRS 154762]

NOTE: IS = ionic strength; Cl = chloride

Figure 6.3.3-3. Ionic Strength, pH, and Chloride Model Predictions versus Topopah Spring Tuff Pore Water Evaporation Data

7.3.3.3.1 Uncertainties in Residual Stress in Outer Lid Closure Welds

As discussed in Section 7.3.3, the closure welds of the outer lid of the waste package outer barrier will be treated by induction heating to mitigate stresses and generate compressive stress at the surface and down to a significant depth. The induction heating treatment will be limited to the closure weld area, and will be performed in such a way that other areas are not heated to undesirable temperatures. The resulting residual stress profiles as a function of depth in the outer closure lid welds were calculated (CRWMS M&O 2000 [DIRS 151564], Section 6.2). As discussed in the *Abstraction of Models of Stress Corrosion Cracking of Drip Shield and Waste Package Outer Barrier and Hydrogen Induced Corrosion of Drip Shield* (CRWMS M&O 2000 [DIRS 151549], Sections 5.3 and 6.3.1.1), the profile with the highest hoop stress from the calculated residual stress profiles was used as a mean stress profile for the outer closure lid weld region. This section provides the technical basis and an approach to quantifying the uncertainty in the calculated mean residual stress. It is assumed in this analysis that the stress measurement uncertainty is the primary contributor to the total uncertainty in the residual stress. Because no stress profile data are available for the waste package design, the uncertainty quantification is based on literature data generated for similar stress mitigation techniques, such as the induction heat treatment process referred to as Induction Heating Stress Improvement (IHSI) (Offer 1983 [DIRS 154454]).

The measurement of residual stresses in components may involve the use of one or more techniques to obtain the total stress state. The techniques used may require the destruction of the component to determine the residual stresses, or they may be performed in a totally nondestructive manner. Because the data generated for IHSI utilized the mechanical (strain gage stress relief) and x-ray residual stress techniques for measurement, these two techniques are therefore the focus of this analysis, and the errors and accuracy associated with those techniques are quantified. Those are two of the most popular residual stress measurement techniques. The x-ray residual stress technique is a nondestructive technique; the strain gage stress relief technique is a destructive technique (Offer 1983 [DIRS 154454]).

X-Ray Diffraction Residual Stress Measurements–The x-ray diffraction technique is the most routinely used nondestructive technique for determining surface residual stresses. It determines the stress by measuring the interplanar spacings in the material. If subsurface residual stresses must be measured, then material can be removed (making this method a destructive technique) and the measurement repeated.

The x-ray technique for measuring residual stress is based on the fact that the lattice spacings (d-spacings) of the atomic planes in a crystalline material are altered by stress. The lattice spacings can be measured by determining the angular position of the diffracted x-ray beam (Bragg's Law). This technique is strictly valid for measurements of stress in a material that is homogeneous, isotropic, and elastic. Wrought austenitic stainless steels and wrought nickel alloys generally meet these requirements.

One of the assumptions made in performing x-ray residual stress measurements is that the penetration depth of the x-ray beam is small, so in the volume being examined, the stress perpendicular to the surface is zero because of the lack of constraint at the surface. For steels and nickel alloys using chromium K-alpha radiation, as used in the evaluations reported for the

and detailed mechanistic modeling will provide useful information to determine the long-term stability of the passive film under repository-relevant exposure conditions.

Previous analyses of Alloy 22 general corrosion were based on data from weight-loss measurements on samples exposed for approximately two years. Because of the low corrosion rates in the material, the data showed significant uncertainties that are due mostly to measurement uncertainty (see Section 7.3.5.2). As a result, the data showed no discernible effects of temperature, environment, or exposure times on corrosion rates. New analyses based on new electrochemical data have been conducted to evaluate the effects of temperature. While the correlation developed is based on limited data over a small temperature range, the model provides a basis for evaluating waste package performance over ranges of time and location in the potential repository.

Potential early failures of waste packages by improper heat treatment are included in the waste package and TSPA analysis. Although the probability of the occurrence is very low, the consequence of improper heat treatment could lead to a gross failure of affected waste packages. The analysis results show that the probability of having at least one waste package improperly heat-treated is 20.2 percent, and the probability of having two waste packages affected is 2.6 percent. The probability of having three waste packages with improper heat treatment is about 0.2 percent. Assuming a total of 100 realizations for the waste package degradation analysis using the WAPDEG model, those probabilities provide that 77 out of 100 realizations would have no waste packages affected by improper heat treatment. Out of 100 realizations, 20 realizations would have at least one waste package affected and 3 realizations would have two waste packages affected.

Based on the additional analyses documented in this report, the following corrosion models and/or parameters are recommended for the waste package degradation analysis:

- Temperature-dependent Alloy 22 general corrosion model II (excluding one outlier from the passive current density data) with the total variance of the general corrosion rates from the weight-loss measurements due to uncertainty and the thermal-hydrologic histories sampled (see Section 7.3.5.3.2)

- The fraction of weld flaws capable of propagation in the radial direction given by a ±3 standard deviation truncated lognormal distribution with a mean of 0.01 and bounded between 0.5 (+3 standard deviations) and 0.0002 (-3 standard deviations) (see Section 7.3.3.3.4)

- The stress threshold for the initiation of stress corrosion cracking given by a uniform distribution between 80 and 90 percent of the Alloy 22 yield strength (see Section 7.3.3.3.3)

Source: DTN: MO0010MWDSUP04.010 [DIRS 152884]

NOTE: Shown in the figure is hoop stress as a function of depth in the Alloy 22 inner closure lid weld region (10-mm thick) using uncertainty bounds at ±5, 10, and 30 percent of the yield strength, along with the lower bound of the threshold stress (80 percent of the yield strength).

Figure 7.4-12 Hoop Stress versus Depth for Inner Closure-Lid Weld Region of Waste Package Outer Barrier for Crack Initiation by Stress Corrosion Cracking

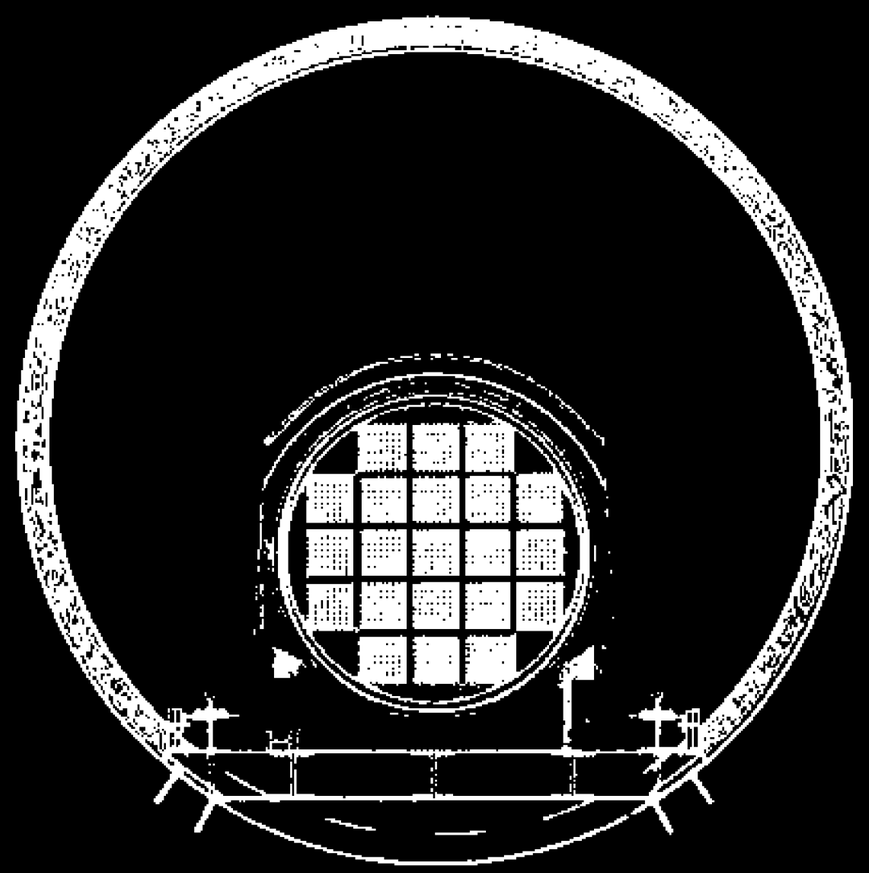

Figure 8.3.2.3.1-1 Main Convection Cells within the FBS

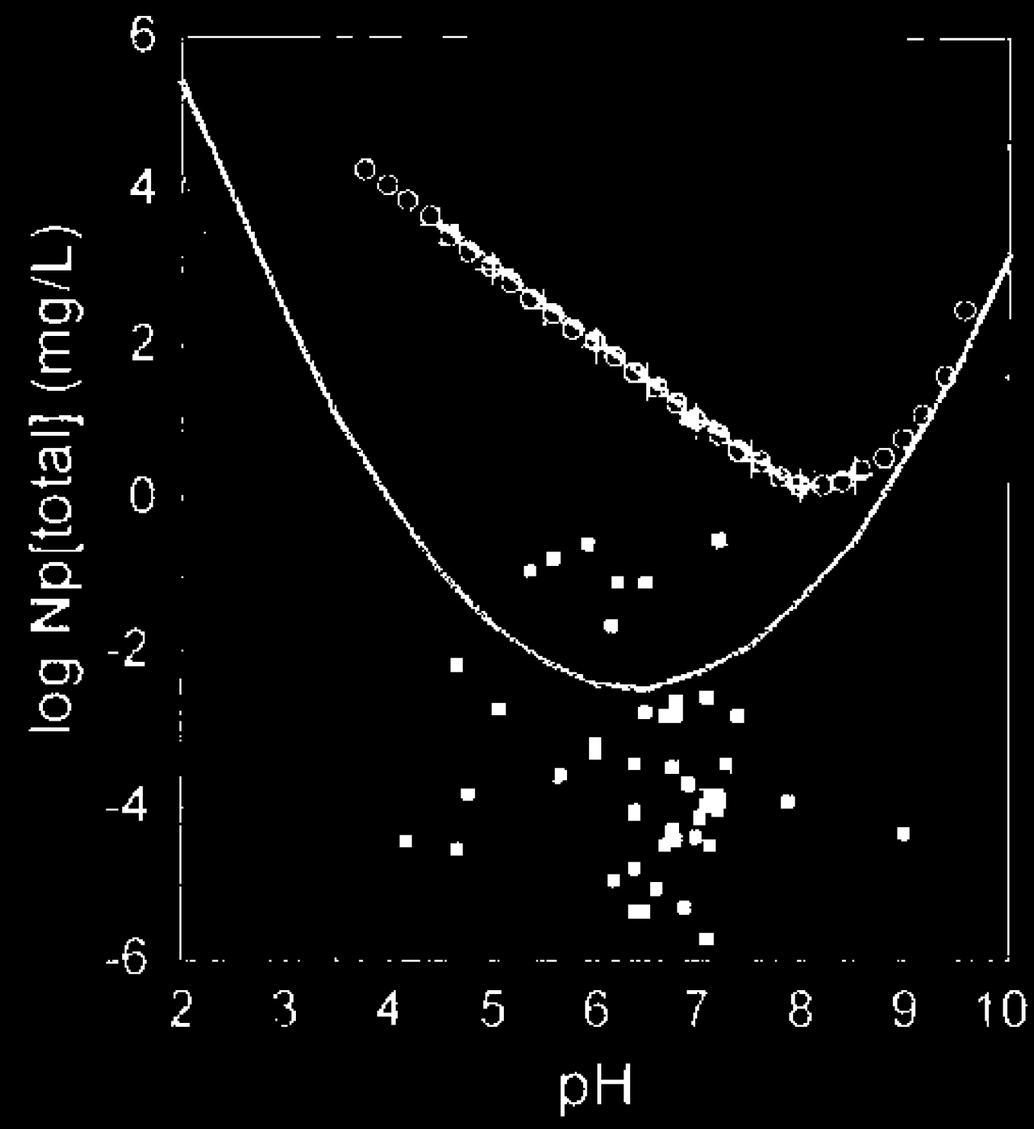

Source: [illegible]

Figure 9-6b Neptunium Dissolved Concentration Limit Models and Data

less than the value predicted by the Philip model, which does not explicitly account for the effects of surface roughness and long-range molecular interactions that increase when water films become very thin. Similarly, the average film velocity is probably much less than that calculated using the Navier-Stokes solution; for example, the Tokunaga et al. (2000 [DIRS 152914]) results show that this approach greatly overestimates film mobility for roughened glass (Figure 10.3.2-2).

10.3.2.3.5 Uncertainties and Limitations

Solutes affect the activity of water in solution and may change the free energy of a thin film. Ionic solutes tend to shorten the length scale for electrostatic interactions, which would affect the free energy for thin films (e.g., less than 1 μm, where adsorption becomes much more important, as discussed previously). Surface tension (against vapor) for aqueous solutions of common salts increases with concentration, but is relatively insensitive (Weast and Astle 1981 [DIRS 100833], p. F-34). By analogy, film behavior may also be relatively insensitive to the effect of solutes. The associated uncertainty in the average velocity of film flow is probably less than that associated with surface roughness heterogeneity.

This discussion is limited to film flow on wettable surfaces, which is generally applicable to metal-oxide surfaces in the EBS. However, there is a possibility that metallic surfaces in the EBS could have nonwetting characteristics, which would tend to decrease film thickness and mobility, but could also induce the formation of droplets. If droplets were in moisture equilibrium with the gas phase, their sizes could range from a few microns to a few millimeters in the relative humidity range of 99 to 99.99 percent or greater. The transport characteristics of such droplets are not addressed here.

Effects of surface heterogeneity produce channeling of flow, as observed by Tokunaga et al. (2000 [DIRS 152914], p. 1743 and Figure 5) in comparing transient film movement on roughened plate glass versus glass cast of a natural fracture surface. The macroscopic average film flow velocity may be increased because movement of thicker films in channels is less hindered by viscous dissipation. Fluid film thickness in channels may be increased by capillarity, depending on the scale of surface roughness. Capillarity was probably important in the results presented by Tokunaga et al. (2000 [DIRS 152914], p. 1740) because the surface exhibited roughness at scales similar to the average film thickness, and because the relative humidity was sufficiently high that the potential equilibrium capillary radius-of-curvature for the film surface was of the same order as the scale of surface roughness.

The Philip approach for estimating film free energy (corresponding to matrix potential) is empirical, based on selection of a functional form to represent available measured data (Philip 1977 [DIRS 152255], Equation 33). The approach would suggest that film free energy increases with absolute temperature (Philip 1977 [DIRS 152255], Equation 34), such that a thicker, more mobile film would form in equilibrium with a given value of relative humidity. However, the surface tension of pure water against air (Weast and Astle 1981 [DIRS 100833], p. F-36), and thus the energy associated with this interface, decreases with increasing temperature. This appears to be inconsistent based on an analogy between liquid-vapor and solid-liquid interactions, and is not supported by empirical data. Thus, the approach is

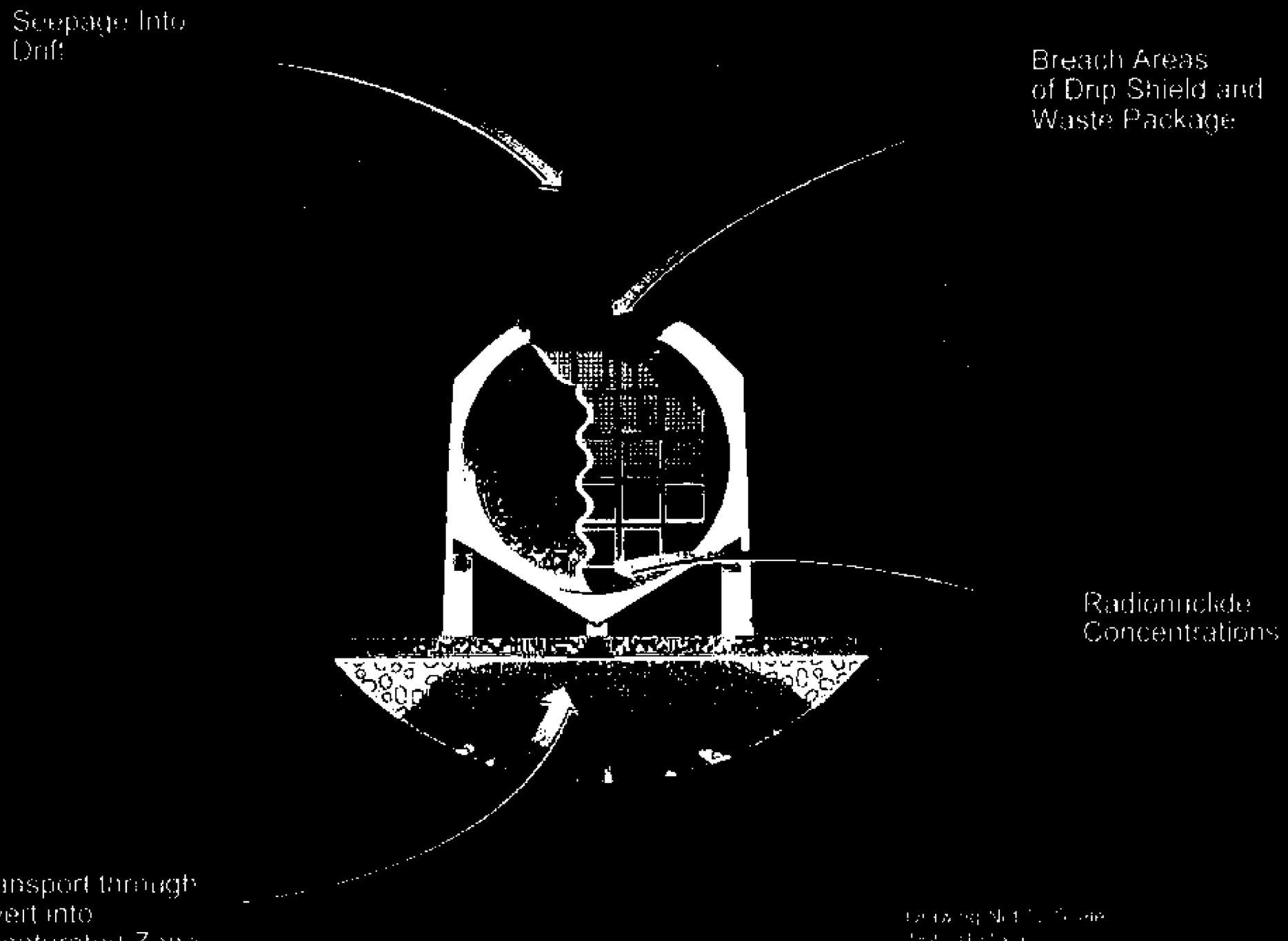

Figure 10.2-1 Conceptualization of an Emplacement Drift after the Drip Shield and Waste Package are Breached and Radionuclides can Transport through the Engineered Barrier System

percolation cases. The simulation results show that for these cases, most of the radionuclide mass still remains in the matrix at breakthrough. Therefore, the effects of the drift shadow model on transport extend beyond the zone of reduced flow beneath the waste emplacement drift and, in some cases, beyond the existing model boundary. The effect of the drift shadow transport model on breakthrough curves at the water table has not been investigated. For radionuclide releases from drifts without seepage, the results presented in this section indicate that transport times to the water table will be thousands to tens of thousands of years. The drift shadow analysis presented is a preliminary and exploratory investigation of flow and transport processes not previously included in process models or TSPA analyses of Yucca Mountain. Further justification in terms of additional analyses and field or laboratory experiments are needed prior to incorporating the complete drift shadow flow and transport analysis into the TSPA baseline.

11.3.2 Matrix Block Discretization and Its Effects on Unsaturated Zone Flow and Transport Simulations

In this section, the effects of matrix block discretization schemes on UZ flow and transport simulations are evaluated.

11.3.2.1 Introduction

Within the context of the continuum approach for modeling flow and transport in unsaturated fractured rock, a numerical gridblock generally includes a fracture block and a matrix block. Depending on the matrix block discretization scheme used for a numerical simulation, the matrix block can be treated as a single matrix gridblock or subdivided into a number of matrix gridblocks. Each matrix gridblock generally corresponds to a matrix continuum.

Because fractures and the matrix have different hydraulic properties, flow and transport between them significantly affects the overall flow and transport behavior in the UZ. Consequently, the accuracy with which flow and transport between them is calculated, which is largely determined by the matrix block discretization scheme, is a critical issue for simulating overall flow and transport processes and for assessing the performance of the potential repository.

As discussed in *Conceptual and Numerical Models for UZ Flow and Transport* (CRWMS M&O 2000 [DIRS 141187], Section 6.4), a dual-permeability model (DKM) has been used as the baseline approach for modeling UZ flow and transport processes. This approach was based on considerations regarding flow and transport behavior in the UZ, the scale of the problem, data availability, and computational feasibility (CRWMS M&O 2000 [DIRS 141187], Section 6.4.2).

Because the matrix is orders of magnitude less permeable than the fracture network, very steep gradients (sharp fronts) may develop in the matrix near fractures. In the DKM, the matrix is treated as a single continuum. As a result, capillary pressure gradients (which drive imbibition) and concentration gradients (which drive diffusion) cannot be fully described. Use of the DKM, therefore, may introduce uncertainty into simulations of UZ flow and transport. To evaluate the effect of the uncertainty, this section compares DKM simulation results to results obtained using the multiple interacting continua (MINC) discretization scheme, which was devised specifically to eliminate this source of uncertainty by using multiple matrix blocks per fracture block (Pruess and Narasimhan 1985 [DIRS 101707], pp. 14 to 16).

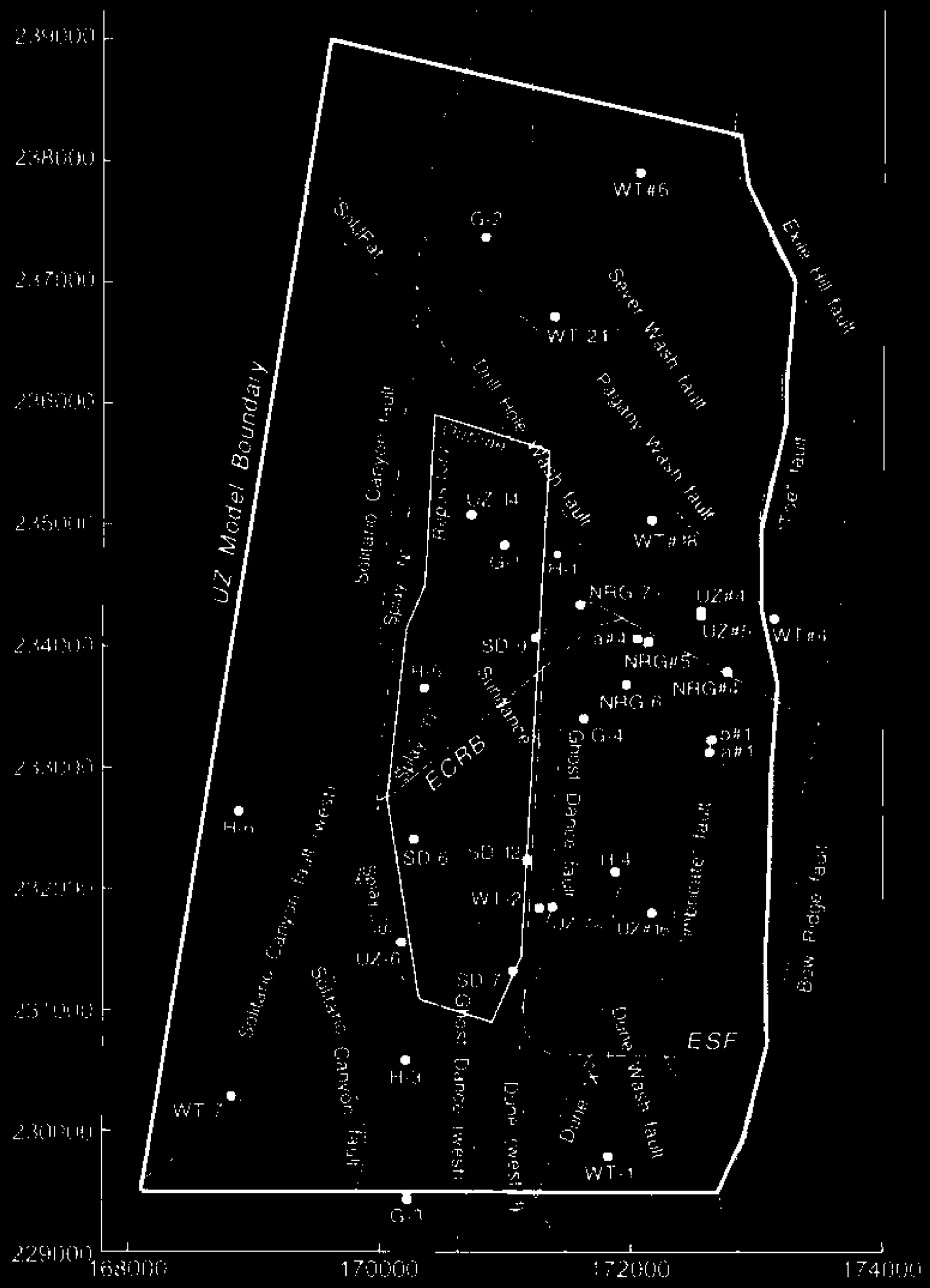

NOTE: The East-West cross section (A-A') was used in numerical simulations.

Source: CRWMS M&O (2000) [DIRS 141187], Figure 1.

Figure 11.3.2-3. Plan View of the Unsaturated Zone Model Domain and the East-West Cross Section

be ruled out is one in which the flowing intervals depicted as single fractures of aperture $2b$ are actually fractured zones of enhanced permeability through which water and radionuclides transport.

To implement such a model, it is possible to use the same mathematical representation as was employed by Sudicky and Frind (1982 [DIRS 105043]), and therefore, the impact of this conceptualization can be examined using the existing particle tracking model by modifying only the parameterization. To do so, the flowing interval spacing was held constant at a mean value of 21 m (CRWMS M&O 2000 [DIRS 154927], p. 13), while adjusting the fracture porosity and, hence, aperture. The fracture porosity in such a medium is a relatively unconstrained parameter that has been sampled over a wide range. For systems with fracture zones rather than individual fractures, it would seem that the fracture porosity could be larger than assumed in previous calculations, perhaps as large as 1 percent. Keeping $2B = 21$ m, the computed aperture for a fracture porosity of 0.01 would be 0.21 m. Referring to Figure 12.3.2.3-7, fracture aperture is computed using simple geometric considerations such that fracture porosity = b/B. This seemingly large aperture value actually represents all of the pore space within the highly fractured zone, that is, the fracture volume and the intrinsic porosity within the intact rock contained in the fractured zone. By assuming that the concentration profile is constant across this zone, which could perhaps be a meter or two in breadth, a void volume equivalent to an aperture of 21 cm is not unreasonable. This parameter should be thought of as a convenience for setting the spacing and fracture porosity as it no longer has the meaning of an aperture when the model is used to represent a flowing network of fracture zones.

The other element of this alternate description of the fracture transport system is the likelihood of sorption within the fractured zones. As opposed to the individual fracture treatment, in which sorption on the faces of fractures is difficult to justify, the alternate model consists of a porous medium within the fracture zones, and retardation due to sorption is easy to justify. In the matrix diffusion model, this sorption is input as a retardation factor within the fracture zone. To set the retardation factors within the fracture zones, it is assumed that the porosity is essentially that of the intact matrix rock and that the same sorption coefficient K_d applies within the fracture zone. Then, the normal relationship between the sorption coefficient and the retardation factor R_f is assumed to apply:

$$R_f = 1 + \rho_b K_d/\theta \qquad \text{(Eq. 12.3.2.3-2)}$$

where

ρ_b = dry bulk density, including pores
θ = porosity

Two sets of simulations were performed using FEHM V2.11 to examine the impact of this alternate conceptual model. The first considers transport of a conservative species such as carbon-14 to the 20-km boundary. All base case parameters are chosen except the fracture porosity, which is set to 0.01 to capture the effect of transport through fracture zones (spaced 21 m apart) rather than through individual fractures. Figure 12.3.2.3-8 compares the breakthrough curves for a release location in region 1 of the saturated-zone footprint. Also shown in this comparison is the same simulation with no matrix diffusion. The adoption of the

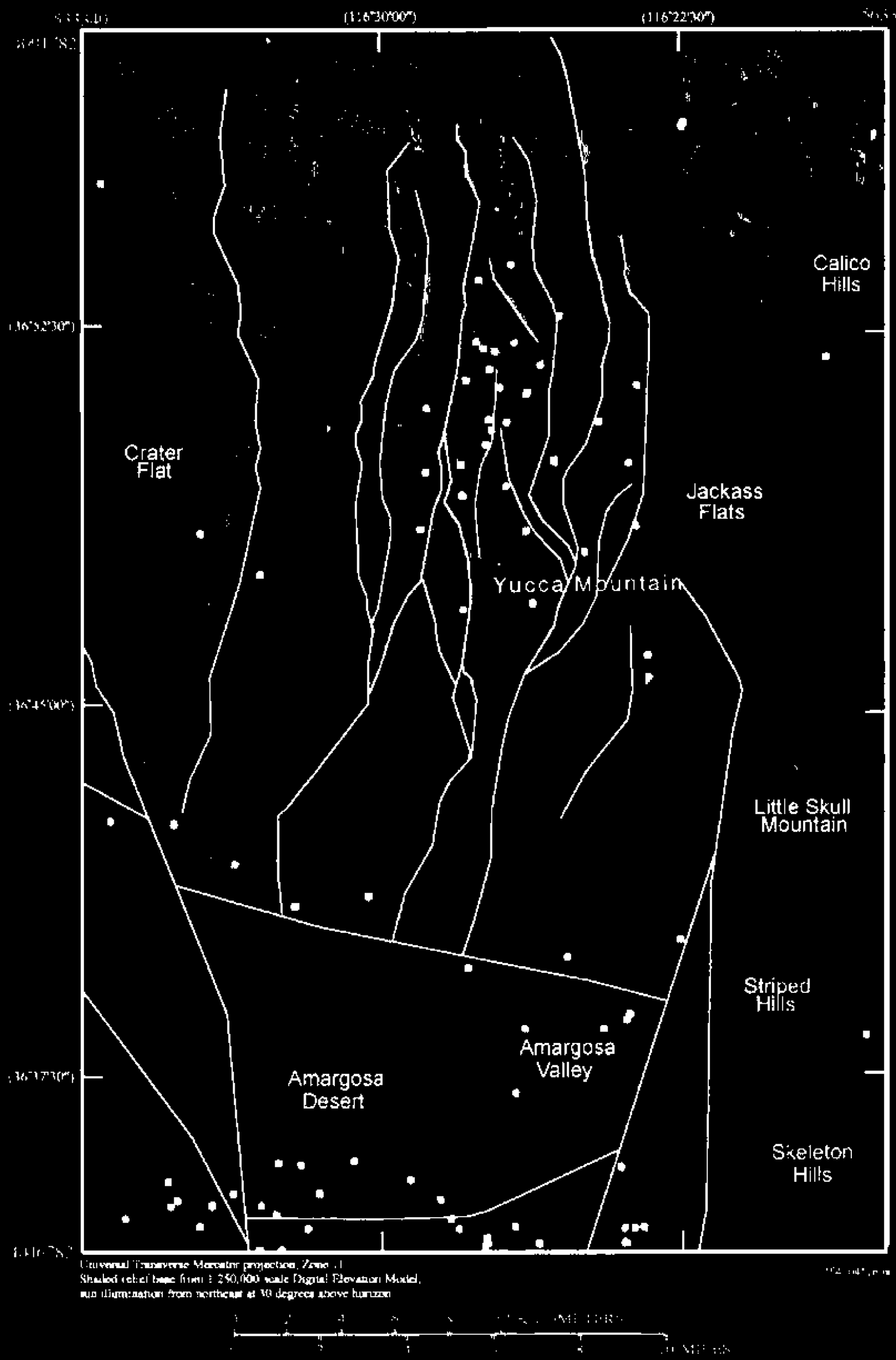

Source: Adapted from USGS 2001 [DIRS 154625], Figure 1-2

Figure 12.2-2. Borehole Locations, Water-Level Altitudes, Potentiometric Surface Contours, and Location of Tertiary Faults in the Site-Scale Saturated Zone Model Area

13.2.1.12 Distribution Fitting to the Stochastic Biosphere Dose Conversion Factors for the Groundwater Release Exposure Scenario

Total System Performance Assessment-Site Recommendation Treatment–The activity documented in *Distribution Fitting to the Stochastic BDCF Data* (CRWMS M&O 2000 [DIRS 144055]) was conducted to derive statistical distributions of the BDCFs. The individual realizations (130 for this approach) for each GENII-S V.1.4.8.5 run were analyzed to ascertain which of several distributions were acceptable for representing the data. The distributions included normal, lognormal, shifted lognormal, and others. The chi-square test was used to determine acceptability of fitting.

Radionuclides that exhibited a change in mean BDCF value of less than 15 percent over the periods of continuing irrigation considered were represented by the distribution derived from the longest period of irrigation. In cases where the change in BDCF mean value was larger than 15 percent over the period of irrigation, the data were further analyzed to incorporate the effect of soil erosion.

Updated Treatment–The updated report (CRWMS M&O 2001 [DIRS 153207]) documented distribution fitting to the updated BDCFs for the groundwater release exposure scenario. The approach to distribution fitting was identical to that presented above. For this iteration, 150 individual model realizations were generated per each GENII-S V.1.4.8.5 run. This increase in sample size improved the treatment of statistical uncertainty inherent in the process.

In the case of carbon-14, none of the distributions considered were deemed to be acceptable; therefore, an empirical distribution was used in the TSPA. The empirical distribution was specified in terms of percentiles at five-percent intervals.

13.2.1.13 Abstraction of Biosphere Dose Conversion Factor Distributions for Irrigation Periods

Total System Performance Assessment-Site Recommendation Treatment–In cases where radionuclide buildup in soils was found to be potentially significant (see Section 13.2.1.12), the BDCF data (see Section 13.2.1.10) were subjected to additional analysis, as documented in *Abstraction of BDCF Distributions for Irrigation Periods* (CRWMS M&O 2000 [DIRS 144054], Section 6). The mean value of the fitted data for each radionuclide was shown to be in the form of an asymptotic exponential function, as expected from the model used by the GENII-S V.1.4.8.5 code for radionuclide loss from decay, leaching, and harvesting. The exponential factor was then modified to include the additional loss mechanism of soil removal, with a characteristic time of 250 years. The overall effect was to reduce the asymptotic (long-term) BDCF value by some degree. For radionuclides with a short buildup time compared to 250 years, the change in BDCF was insignificant. However, in cases where the predicted radionuclide buildup was long compared to 250 years, the effect was significant. In all cases, the long-term, and therefore conservative, values of BDCFs were used in the TSPA. This conservative approach eliminated the need to define and justify a representative distribution for the number of years that various plots of land associated with the hypothetical community had been subject to continuing (or sporadic) irrigation and production.

values of mass loading that correspond to differences in predicted ash depth at the location of the receptor.

Another parameter important in the biosphere modeling for the volcanic eruption was the thickness of ash layer at the location of interest. The thickness of the ash layer that could be deposited 20 km from the potential repository was uncertain (CRWMS M&O 2000 [DIRS 153246], Section 3.10.5.1). The median eruptive event was predicted to produce an ash layer less than 1 cm thick 20 km downwind. The minimum ash layer calculated for the midpoint of the plume at 20 km was less than 0.1 mm, corresponding to a relatively small eruption that produces only a dusting of ash at that distance. The maximum ash layer was 36 cm, corresponding to a large eruption that produces a major ash fall covering a large area (CRWMS M&O 2000 [DIRS 153246], Section 3.10.5.1).

Because of the wide range of ash thicknesses, transition-phase BDCFs were developed for two different thicknesses of ash: 1 cm, representing the more likely conditions, and 15 cm, representing thicker ash deposits. The thicker ash layer was chosen to be 15 cm because this thickness corresponds to the depth of surface soil constituting the plant growing zone (it was assumed that 100 percent of a plant's roots were in the surface soil layer) (CRWMS M&O 2001 [DIRS 152434], Sections 6.4.1 and 6.4.4), which is one of the input parameters in GENII-S V.1.4.8.5. Greater thicknesses do not have a significant effect on the calculation outcome because it was assumed that plant roots do not extend past 15 cm in depth. The BDCFs for the steady-state phase use the 15-cm thickness for the ash or soil layer.

Taking into consideration the possible combinations of mass loading and ash thicknesses, the following sets of BDCFs were developed:

- Transition-phase, 1 cm ash layer and annual average mass loading
- Transition-phase, 1 cm ash layer and 10-year average mass loading
- Transition-phase, 15 cm ash layer and annual average mass loading
- Transition-phase, 15 cm ash layer and 10-year average mass loading
- Steady-state phase.

BDCFs were calculated in a series of GENII-S V.1.4.8.5 simulations for each of the 17 radionuclides. Each simulation resulted in 150 model realizations. These results were converted into discrete cumulative probability distributions, which were used in the TSPA with other input parameters to evaluate expected annual doses following a volcanic eruption.

Table 13.4-10 gives the summary of the BDCF calculations for the volcanic eruption. The table includes the means, standard deviations, minimums, and maximums for the BDCFs. The BDCFs for selenium-79 and neptunium-237, calculated after revision of the *Disruptive Event Biosphere Dose Conversion Factor Analysis* (CRWMS M&O 2001 [DIRS 152536]), can be found in Tables 13.3-19 and 13.3-20, respectively. For most radionuclides, BDCFs differ between the scenarios under consideration. The highest BDCFs were for the transition phase, 1-cm ash layer and the annual average mass loading. This set of BDCFs can be compared with the transition-phase BDCFs for a 15-cm ash layer and annual average mass loading. The reason for the difference is that in the 1-cm contaminated ash layer, radionuclides are concentrated in the upper soil. Therefore, the activity concentration in air from resuspended contaminated material

14.3.3.2.4 Scaling Factor for Releases from Waste Packages Hit in the Igneous Intrusion Groundwater Transport Scenario

Conceptually, an approximation of igneous intrusion groundwater transport releases from alternative thermal operating modes could be estimated by multiplying the releases reported in the S&ER by a scaling factor equal to the waste package density (number of waste packages per acre of repository area) for the thermal operating mode described in the S&ER (DOE 2001 [DIRS 153849]) divided by the waste package density in the alternative. However, significant revisions to key disruptive events AMRs and calculations were accomplished after the S&ER was finalized. Because of the cumulative impact of these revisions, a simple scaling factor cannot be applied to estimate the approximate magnitude of the release for alternative thermal operating modes.

14.3.3.3 Contribution to Release of Zones 1 and 2 in the Igneous Intrusion Groundwater Transport Model

The new work presented in this section was performed to reduce uncertainty in the impacts of releases from different damage zones associated with the igneous intrusion groundwater transport scenario. Information on the contribution to waste release from different damage zones will support focusing analyses on those areas where uncertainty exists and may be reduced by further analysis. The analysis in this section supports a sensitivity analysis in Volume 2 (McNeish 2001 [DIRS 155023]).

The initial version of *Igneous Consequence Modeling for the TSPA-SR* addressed igneous intrusion groundwater transport consequence modeling for a repository thermal operating mode that included backfill (CRWMS M&O 2000 [DIRS 139563]). An update of this report addresses igneous consequence modeling for an operating mode with no backfill (CRWMS M&O 2000 [DIRS 151560]). The effect that a dike (or dikes) intersecting emplacement drifts has on waste package damage in the igneous intrusion groundwater transport scenario varies with proximity to the dike (CRWMS M&O 2000 [DIRS 151552]). Waste package damage in Zone 1 consists of the area immediately around the dike/drift intersection. Waste package behavior in Zone 1 for the backfill and no-backfill operating modes is bounded by the conservative assumption that three packages on either side of the dike, plus a minimum of one package in the path of the dike (seven total packages minimum, depending on dike width), are sufficiently damaged that they provide no further protection for the waste. For multiple dikes in an event (dike swarm), there are seven waste packages damaged in Zone 1 for each dike.

In an update to *Dike Propagation Near Drifts* (CRWMS M&O 2000 [DIRS 151552]), a Zone 2 region is introduced for the no-backfill thermal operating mode described in the S&ER (DOE 2001 [DIRS 153849]). Zone 2 is defined as the portion of an emplacement drift that has been crossed by a dike and is not included in Zone 1. In the absence of backfill, the waste packages in these drifts are directly exposed to a shock wave and pyroclastic flow resulting from the dike encountering the relatively lower pressure in the repository. Pressure in the emplacement drifts would likely have to rise to lithostatic before the dike could continue to propagate upward. The combination of high temperature (1,040° to 1,170°C) and high pressure (approaching the magmatic lithostatic pressure of 7.5 Mpa at the repository depth) would likely be sufficient to cause some degree of failure of the waste packages in Zone 2. The degree of

The minimum-alluvium sensitivity analysis is implemented in the site-scale saturated zone flow and transport model by reducing the extent of the alluvium uncertainty zone to zero.

Sorption Coefficient in Alluvium for Iodine and Technetium–Further analysis of batch sorption data of technetium-99 and iodine-129 (as TcO_4^- and I^-) onto alluvium samples, as well as recent technetium-99 and iodine-129 column test results, indicate that sorption distribution (K_d) values for technetium-99 and iodine-129 sorbing onto the alluvium are zero under oxidizing (ambient) conditions. Therefore, sorption coefficients in the alluvium for iodine and technetium were considered to be zero in the saturated zone transport model.

Sorption Coefficient in Alluvium for Neptunium and Uranium–New results from two column experiments for K_d values for neptunium-237 in the alluvium have been performed in which the effective K_d values of neptunium-237 were significantly lower than values measured in batch sorption experiments with the same material used to pack the columns. Therefore, the probability distribution for neptunium sorption coefficient in the alluvium was changed from a probability distribution based on laboratory batch experiments to one that represents batch and column laboratory experiments. The distribution function gives considerable weight to the column experiments, which weights the lower sorption-coefficient values. Based on the absence of experimental data on uranium sorption coefficients in alluvium, the probability distribution for uranium is represented as the sorption-coefficient probability distribution for neptunium in the alluvium.

Sorption Coefficient for Neptunium in Volcanic Tuffs–The probability distribution used for the neptunium sorption coefficient in the matrix was changed from a probability distribution based on a vitric rock type to a probability distribution that is more representative of the rock types that the flow path will encounter. For a given set of realizations (i.e., simulations with Monte Carlo sampling) the new probability distribution is determined by sampling the vitric distribution approximately 67 percent of the time and the zeolitic distribution 33 percent of the time.

K_c (Reversible Colloids) Model for Groundwater Colloid Concentrations–The sensitivity analysis for the saturated zone consists of simulation of radionuclide breakthrough curves for the two classes of radionuclides associated with the reversible colloid model: strongly sorbing radionuclides (plutonium, americium, and thorium) and moderately sorbing radionuclides (strontium, cesium, and protactinium). These simulations are implemented in the site-scale saturated zone flow and transport model using resampled values for the K_c parameter and for the K_d of strongly sorbing radionuclides. The values for the K_c parameter used in this analysis are based on sampling of uncertainty distributions for the K_d of americium onto colloids and for the concentration of colloids in the groundwater, as explained in Volume 2 (McNeish 2001 [DIRS 155023], Section 3). The uncertainty distribution for K_d of strongly sorbing radionuclides onto the alluvium material is changed to beta distribution with greater statistical mass near the expected value of 50 ml/g (McNeish 2001 [DIRS 155023], Section 3). Other stochastic parameters for the saturated zone have the same values for the sensitivity analysis as the SSPA Volume 2 (McNeish 2001 [DIRS 155023]) supplemental analysis.

Enhanced Matrix Diffusion–For this case, most of the rock matrix in the volcanic units is available for radionuclide storage and sorption in the transport process in most of the

152354 Cragnolino, G.A.; Dunn, D.S.; Brossia, C.S.; Jain, V.; and Chan, K.S. 1999. *Assessment of Performance Issues Related to Alternate Engineered Barrier System Materials and Design Options.* CNWRA 99-003. San Antonio, Texas: Center for Nuclear Waste Regulatory Analyses. TIC: 248875.

152434 CRWMS M&O 2001. *Environmental Transport Parameter Analysis.* ANL-MGR-MD-000007 REV 00 ICN 01. Las Vegas, Nevada: CRWMS M&O. ACC: MOL.20010208.0001.

152435 CRWMS M&O 2000. *Transfer Coefficient Analysis.* ANL-MGR-MD-000008 REV 00 ICN 02. Las Vegas, Nevada: CRWMS M&O. ACC: MOL.20001016.0005.

152438 CRWMS M&O 2000. *Input Parameter Values for External and Inhalation Radiation Exposure Analysis.* ANL-MGR-MD-000001 REV 01 ICN 00. Las Vegas, Nevada: CRWMS M&O. ACC: MOL.20001122.0005.

152446 ICRP (International Commission on Radiological Protection) 1996. *Age-Dependent Doses to Members of the Public from Intake of Radionuclides: Part 5 Compilation of Ingestion and Inhalation Dose Coefficients.* Volume 26, No. 1 of *Annals of the ICRP.* Smith, H., ed. ICRP Publication 72. New York, New York: Pergamon Press. TIC: 235870.

152447 ICRP (International Commission on Radiological Protection) 2000. *Radiation Protection Recommendations as Applied to the Disposal of Long-lived Solid Radioactive Waste.* Volume 28, No. 4 of *Annals of the ICRP.* Valentin, J., ed. ICRP Publication 81. New York, New York: Pergamon Press. TIC: 249031.

152496 CRWMS M&O 2000. *GVP Software Routine Report.* SDN: 10341-SRR-1.02-00. Las Vegas, Nevada: CRWMS M&O. ACC: MOL.20000908.0038.

152499 CRWMS M&O 2000. *SCCD Software Routine Report.* SDN: 10343-SRR-2.01-00. Las Vegas, Nevada: CRWMS M&O. ACC: MOL.20010205.0113.

152517 CRWMS M&O 2001. *Evaluate Soil/Radionuclide Removal by Erosion and Leaching.* ANL-NBS-MD-000009 REV 00 ICN 01. Las Vegas, Nevada: CRWMS M&O. ACC: MOL.20010214.0032.

152536 CRWMS M&O 2001. *Disruptive Event Biosphere Dose Conversion Factor Analysis.* ANL-MGR-MD-000003 REV 01. Las Vegas, Nevada: CRWMS M&O. ACC: MOL.20010125.0233.

152539 CRWMS M&O 2001. *Nominal Performance Biosphere Dose Conversion Factor Analysis.* ANL-MGR-MD-000009 REV 01. Las Vegas, Nevada: CRWMS M&O. ACC: MOL.20010123.0123.

The initial selection of bit type is typically made on the basis of what is known about the formation characteristics. The terms usually used by drilling engineers to describe the formation characteristics are drillability and abrasiveness. The drillability of the formation is a measure of how easy the rock formation is to drill. It is inversely related to the compressive strength of the rock, although other factors are also important. The abrasiveness of the formation is a measure of how rapidly the cutting surface of a bit will wear when drilling the formation. Although there are some exceptions, the abrasiveness tends to increase as the drillability decreases (Bourgoyne et al. 1986 [DIRS 155233]).

The bases for these discussions are typical practices used in drilling water wells in southwestern United States. The International Association of Drilling Contractors (IADC 1992 [DIRS 155232]) has developed a classification chart for selection of roller bits. Using this classification chart, roller bits with characteristics of 7-1 or 7-2 (hard semi-abrasive and abrasive formations) would be selected for drilling through the welded geologic units at Yucca Mountain, based on geo-mechanical properties. The 7-1 roller drill bits utilize 80 to 90 degree short chisel tungsten-carbide inserts, whereas the 7-2 roller drill bits utilize 60 to 70 degree short projectile tungsten-carbide inserts. Roller bits are typically used in drilling water wells due to their low cost and wide range of operational flexibility. Polycrystalline diamond cutter and diamond cutter drag bits typically are not used in water well drilling because of the high costs of these drill bits. Direct circulation hammer drills are sometimes used to drill brittle competent rock such as welded volcanic tuff, but they typically are inefficient in unconsolidated alluvium or incompetent rock formations. This limitation reduces the use of these drills in typical water well drilling. However, the discussions provided herein would be generally applicable to roller or hammer bits.

Uniaxial compressive strengths for the major geologic units at Yucca Mountain were determined using confined compression tests (Table A-1). Static Young's Modulus values were computed from stress-strain data obtained from unconfined compression tests. The intact rock unconfined compressive strength and elastic modulus by rock unit are given in Table A-1.

Based on the design described in the *Yucca Mountain Science and Engineering Report* (DOE 2001 [DIRS 153849]), Titanium grades 7 and 24 are candidate materials for drip shield fabrication and Alloy 22 and 316 nuclear grade stainless steel are candidate materials for waste package fabrication (DOE 2001 [DIRS 153849] Sections 2.4.4 and 3). Physical and chemical properties for these materials have been determined, and the tensile strength and modulus of elasticity for candidate drip shield and waste package materials are shown in Table A-2.

There have been a number of studies conducted to correlate operational parameters to rate of penetration of the drill bit. Many of these studies indicate that the rate of penetration is inversely proportional to the square of the compressive strength of the material being drilled, all other factors being equal (Bourgoyne et al. 1986 [DIRS 155233]; Warren 1987 [DIRS 155234]). This would indicate that a change of approximately 1.4 in the compressive strength of the material would be adequate to produce the factor of two change in the rate of penetration necessary for recognition by a driller.